https://doi.org/10.5194/acp-2021-345
Preprint. Discussion started: 29 April 2021

Atmospheric Chemistry and Physics Discussions

Water vapor anomaly over the tropical western Pacific in El Niño winters from radiosonde and satellite observations

Minkang Du[1,2,3] Kaiming Huang[1,2,3] Shaodong Zhang[1,2] Chunming Huang[1,2]

Yun Gong[1,2] and Fan Yi[1,2,3]

[1]School of Electronic Information, Wuhan University, Wuhan, China

[2] Key Laboratory of Geospace Environment and Geodesy, Ministry of Education, Wuhan, China

[3]State Observatory for Atmospheric Remote Sensing, Wuhan, China

Correspondence: Kai Ming Huang (hkm@whu.edu.cn)

https://doi.org/10.5194/acp-2021-345
Preprint. Discussion started: 29 April 2021

Atmospheric Chemistry and Physics Discussions

Abstract. Using radiosonde observations at five stations in the tropical western Pacific and reanalysis data for 15 years from 2005 to 2019, we report an extremely negative anomaly in atmospheric water vapor during the super El Niño winter of 2015/16, and compare the anomaly with that in the other three El Niño winters. Strong specific humidity anomaly is concentrated below 8 km of the troposphere with a peak at 2.5-3.5 km, and column integrated water vapor mass anomaly over the five radiosonde sites has a large negative correlation coefficient of -0.63 with oceanic Niño3.4 index, but with a lag of about 2-3 months. In general, the tropical circulation anomaly in the El Niño winter is characterized by divergence (convergence) in the lower troposphere over the tropical western (eastern) Pacific, thus the water vapor decreases over the tropical western Pacific as upward motion is suppressed. The variability of the Hadley circulation is quite small and has little influence on the observed water vapor anomaly. The anomaly of the Walker circulation makes a considerable contribution to the total anomaly in all the four El Niño winters, especially in the 2006/07 and 2015/16 eastern-Pacific (EP) El Niño events. The monsoon circulation shows a remarkable change from one to the other event, and its anomaly is large in the 2009/10 and 2018/19 central-Pacific (CP) El Niño winters and small in the two EP El Niño winters. The observed water vapor anomaly is caused mainly by the Walker circulation anomaly in the supper EP event of 2015/16 but by the monsoon circulation anomaly in the strong CP event of 2009/10. Owing to the anomalous decrease in upward transport of water vapor during the El Niño winter, less cloud amount and more outgoing longwave radiation over the five stations are clearly presented in satellite observation.

1 Introduction

Water vapor is a variable trace composition of the atmosphere, whereas it has a profound impact on global energy budgets not only through latent heat release upon phase transitions (Held and Soden, 2000),

https://doi.org/10.5194/acp-2021-345
Preprint. Discussion started: 29 April 2021

but also through cloud formation that reflects long-wave radiation from below and short wave radiation from above (Stevens et al., 2017), thus water vapor plays a substantial role in the climate system as a dominant greenhouse gas in the troposphere. The tropical Pacific is a major convection center and abundant water vapor region. Sea surface temperature (SST) anomaly in the tropical Pacific has an important influence on water vapor transport, cloud cover and precipitation distribution due to the tropical circulation changes caused by El Niño-Southern Oscillation (ENSO). ENSO is characterized by anomalous SST in the tropical Pacific. During ENSO, there is significant precipitation variability in the Euro-Mediterranean (López-Parages and Rodríguez-Fonseca, 2012), Middle East (Sandeep and Ajayamohan, 2018), southwest central Asia (Mariotti, 2007), western Africa (Okazaki et al., 2015), Pacific Ocean (Quartly et al., 2000) and America (Lee et al., 2014). ENSO has an effect on seasonal rainfall in East Asian by inducing a weaker and later onset of the Indian monsoon circulation (Dai and Wigley, 2000; Zhao et al., 2010; Yan et al., 2018). Vertical cloud anomalies in the tropical Atlantic from Aqua Moderate Resolution Imaging Spectroradiometer are linked to ENSO-induced shift and weakening of the Walker circulation and Hadley cell near the equator (Madenach et al., 2019). The strong 1997/98 El Niño resulted in cloud structure anomalies and their radiative property changes over the tropical Pacific (Sun et al., 2012), and increased upper tropospheric cirrus over the mid-Pacific but decreased cirrus over Indonesia (Massie et al., 2000). Numerical investigation also indicated that warm water volume transport and precipitation change are associated with ENSO (Ishida et al., 2008; Hill et al., 2009).

El Niño is generally classified into central-Pacific (CP) El Niño, also known as El Niño Modoki, and eastern-Pacific (EP) El Niño based on distinct spatial distributions of warming SST anomaly averaged over the Niño4 and Niño3 regions (Ashok et al., 2007; Yu and Kao, 2009; Yeh et al., 2009), respectively.

https://doi.org/10.5194/acp-2021-345
Preprint. Discussion started: 29 April 2021

The 2006/07 and 2015/16 events are the EP El Niño because of the stronger SST anomaly during the boreal winter (December to February, as DJF) in the Niño3 region than in the Niño4 region, while correspondingly, the 2009/10 and 2018/19 events are categorized as the CP El Niño (Yeh et al., 2009). The two types of El Niño have different effects on precipitation, surface temperature, moisture transport and carbon cycle over many parts of the world (Weng et al., 2008; Kug et al., 2009; Wang et al., 2013; Yeh et al., 2014; Gu and Adler, 2016; Wang et al., 2018). Su and Jiang (2013) and Takahashi et al. (2013) suggested that water vapor anomaly over the tropical ocean is mainly controlled by thermodynamic process during the 2006/07 EP El Niño, but by both dynamic and thermodynamic processes during the 2009/10 CP El Niño.

The EP El Niño in 2015/16 winter is one of the strongest ENSO events on record. Compared to the strong 1982/83 and 1997/98 El Niños, the 2015/16 El Niño shows distinct aspects that the largest SST anomalies are extended toward the central Pacific (Paek et al., 2017; L'Heureux et al., 2017). As the unusual characteristics, the global effects of the 2015/16 event have attracted much attention. Palmeiro et al. (2017) proposed that an early stratospheric final warming over the polar region and anomalous precipitation over southern Europe in 2016 were related to the 2015/16 super El Niño. Li et al. (2018) revealed that the combined effect of the 2015 ENSO warm phase and Madden-Julian Oscillation (MJO)-4 index negative phase caused a significant deficit of precipitation on the Canadian Prairies in May and June 2015. A striking freshwater anomaly was observed in the equatorial Pacific during the onset of 2015/16 event (Gasparin and Roemmich, 2016), and rainfall $\delta^{18}O$ in the southern Papua was generally enriched by 1.6‰–2‰ during the 2015 El Niño than during the 2013/14 ENSO-normal period (Permana et al., 2016). Owing to convection anomaly during the 2015/16 El Niño, water vapor in the tropical lower stratosphere was increased by hydration of the lower stratosphere through convectively

https://doi.org/10.5194/acp-2021-345
Preprint. Discussion started: 29 April 2021

Atmospheric Chemistry and Physics Discussions

detrained cloud ice (Avery et al., 2017), and quasi-biennial oscillation in the tropical stratospheric wind was disrupted because of dramatic relocation of deep convection (Dunkerton, 2016; Newman et al., 2016). Hence, the 2015/16 El Niño has the important influences on the circulation and composition transport and the mass exchange between the troposphere and stratosphere. In this paper, we investigate water vapor anomaly over the tropical western Pacific in the CP and EP El Niño events from radiosonde and satellite observations, in particular, extreme anomaly in the 2015/16 super El Niño winter, and explore the contributions of the tropical Hadley, Walker and monsoon circulation changes to the observed water vapor anomalies in the different El Niño events.

The data used are briefly described in section 2. In section 3, water vapor anomalies in four El Niño winters are presented, and the relationship between the ENSO intensity and the water vapor anomaly at the observational stations is discussed. In section 4, we decompose the tropical circulation into the Hadley, Walker and monsoon circulation components, and estimate the roles of these circulations in the water vapor variation. Tropical cloud and outgoing longwave radiation (OLR) are investigated in section 5, and a summary is provided in section 6.

2. Data

In present study, we investigate the atmospheric water vapor by using radiosonde observations at five tropical stations for 15 years from January 2005 to December 2019, which are provided by the national oceanic and atmosphere administration (NOAA) at the website of ftp://ftp.ncdc.noaa.gov/pub/data/ua/rrs-data/. The five radiosonde stations are at Koror (7.33°N, 134.48°E), Yap (9.48°N, 138.08°E), Guam (13.55°N, 144.83°E), Truk (7.47°N, 151.85°E) and Ponape (6.97°N, 158.22°E), located in the western Pacific warm pool. Balloon was launched twice daily at 0000

https://doi.org/10.5194/acp-2021-345
Preprint. Discussion started: 29 April 2021

Atmospheric Chemistry and Physics
Discussions
Open Access

UT and 1200 UT, and during balloon ascent, sensing payload on balloon can obtain many meteorological parameters, such as atmospheric pressure, temperature, relative humidity, and wind speed and direction. We plot daily temperature, relative humidity, and wind speed time series observed by radiosonde to identify potential outliers, and then the high resistant asymmetric biweight technique is applied to weed out the outliers (Lanzante, 1996). The radiosonde data is linearly interpolated to a vertical grid of 50 m, and the interpolated data below 10 km is utilized to analyze the atmospheric water vapor variation. Burst height of balloon is usually more than 30 km, thus the data availability below 10 km is high. In the period that we focus on, the data are missing for about 4, 2, 1 and 4 months over Yap, Guam, Truk and Ponape, respectively, and they are almost entirely from the several gaps of observations.

Specific humidity can be derived from the profile of meteorological parameters observed by radiosonde. The saturated vapor pressure e_s is calculated according to a modified version of the Magnus formula as follows (Murray, 1967),

$$e_s = 6.1078 \times \exp\left[\frac{17.269(T - 273.16)}{T - 35.86}\right] \quad (1)$$

where T is the temperature in units of K. And then, the specific humidity q (g kg^{-1}) is determined from the following equations,

$$e = RH \times e_s \quad (2)$$

$$q = \frac{0.622e}{p - 0.378e} \quad (3)$$

where e is the vapor pressure; RH is the relative humidity; and p is the pressure with units of hPa.

In addition, we use the monthly specific humidity, horizontal winds from surface to 300 hPa during the period of 2005-2019, obtained from the European centre for medium-range weather forecasts (ECMWF) ERA5 reanalysis data, to investigate the water vapor anomaly and tropical atmospheric

https://doi.org/10.5194/acp-2021-345
Preprint. Discussion started: 29 April 2021

Atmospheric Chemistry and Physics Discussions

circulation in the region of the radiosonde stations. The reanalysis data is produced by a sequential 4D variational data assimilation scheme, with a latitudinal and longitudinal resolution of 0.25°×0.25° at 37 pressure levels from 1000 to 1 hPa (Hersbach et al., 2020). The data is available at the website of https://cds.climate.copernicus.eu/cdsapp#!/home/.

Oceanic Niño index (ONI) is applied to discuss the correlation between the ENSO and the observed water vapor anomaly. ONI is the measurement of ENSO strength, which is provided by the NOAA at https://catalog.data.gov/dataset/climate-prediction-center-cpcoceanic-nino-index/. The ONI is defined as a 3-month moving average of extended reconstructed sea surface temperature (ERSST) V5 sea surface temperature anomalies in the Niño3.4 region at 5°N-5°S and 120°-170°W (Huang et al., 2017).

Cloud occurrence probability and OLR flux are also examined since they are sensitive to water vapor variation (Stevens et al., 2017; Soden et al. 2008). The OLR data is measured by the NOAA-18 satellite. We use the monthly OLR data between 2005 and 2019 from the NOAA archives with a latitudinal and longitudinal grid of 2.5°×2.5° (Liebmann and Smith, 1996), which can be accessed through the website of https://www.esrl.noaa.gov/psd/data/gridded/data.interp_OLR.html/. Cloud-aerosols lidar and infrared pathfinder satellite observations (CALIPSO) are able to clearly identify cloud vertical structure (Winker et al., 2007). Here, we use the CALIPSO Version 1.00 lidar level 3 cloud occurrence monthly data in a latitudinal and longitudinal grid of 2°× 2.5° with an altitude resolution of 60 m above the mean sea level, and the available data is from June 2006 to December 2016, downloaded from the website of the national aeronautics and space administration (NASA) at https://eosweb.larc.nasa.gov/project/calipso/cloud_occurrence_table/.

3 Water Vapor Anomaly

https://doi.org/10.5194/acp-2021-345
Preprint. Discussion started: 29 April 2021

3.1 Water Vapor Anomaly during El Niño Winter

We derive the profile of specific humidity from the radiosonde observations according to Eqs. (1-3), and then calculate the monthly mean specific humidity. The monthly mean specific humidities in all the same months are further averaged to obtain the monthly climatic normal, thus the monthly mean water vapor anomaly is determined from the monthly mean series by subtracting the corresponding month climatic normal. Figure 1 shows the monthly mean specific humidity anomaly based on the radiosonde observations at Koror, Yap, Guam, Truk and Ponape from January 2005 to December 2019. Atmospheric water vapor is mainly concentrated below 8 km, thus the large water vapor anomaly also occurs below 8 km. It can be seen from Fig. 1 that the water vapor anomaly is remarkably negative over the five stations in the super El Niño winter of 2015-2016. The negative anomaly in the water vapor reaches the peak values of -2.06 g kg^{-1} around 3 km in January at Koror, -3.2 g kg^{-1} around 3 km in February at Yap, -2.39 g kg^{-1} around 2.5 km in January at Guam, -2.29 g kg^{-1} around 3.5 km in February at Truk and -2.66 g kg^{-1} around 2.5 km in February at Ponape, respectively. In the 2006/07, 2009/10 and 2018/19 El Niño winters, the observed water vapor anomalies also exhibit negative throughout the lower troposphere. Hence, the El Niño events can lead to the obvious reduction of water vapor in the region.

With the help of the ERA5 reanalysis data, we investigate the distribution of the abnormal water vapor during the four El Niño events. Here, we introduce an important scalar of column integrated water vapor mass (CWV), also called precipitable water, which is expressed as (Viswanadham, 1981),

$$Q = \frac{1}{g}\int_{p_z}^{p_0} q dp \tag{4}$$

where Q is the CWV in units of kg m^{-2}; $g = 9.8$ m s^{-2} is the acceleration due to gravity; and the pressures p_0 and p_z denote the bounds of integration, respectively. Considering that atmospheric water vapor is mainly distributed below 8 km in the tropics due to the rapid decrease of water vapor with height (Mapes et al., 2017), we choose $p_0 = 1000$ hPa on the ground and $p_z = 300$ hPa corresponding to a height of about 9 km. According to Eq. (4), we calculate the CWV between 30°S and 30°N from January 2005 to December 2019 based on the reanalysis data. Similarly, the monthly mean CWV and its anomaly can be derived from the CWV series. Figure 2 presents the mean CWV anomalies in the four El Niño winters. In the 2006/07 and 2015/16 EP El Niño events, the positive CWV anomalies appear in the equatorial central and eastern Pacific, while in 2009/10 and 2018/19 CP El Niño events, the positive anomalies concentrate in the central Pacific. This is consistent with previous studies (Kug et al., 2009; Takahashi et al., 2013; Xu et al., 2017). The negative anomalies occur in the tropical western Pacific and some tropical latitudes off the equator in both hemispheres. In the region of the five radiosonde stations, the CWV anomaly is evidently negative and comparable between the 2009/10 and 2015/16 events although the two events are classified into different El Niño types. Whereas in the other two events, the water vapor anomaly is weak, which is in rough agreement with the radiosonde observation in Fig. 1.

3.2 Relation between CWV Anomaly and ONI

We choose the reanalysis CWV anomalies at the five radiosonde stations to discuss the relationship between the water vapor anomaly and the ENSO. The monthly mean CWV anomaly averaged at the five stations is derived from the radiosonde and reanalysis data from January 2005 to December 2019. Considering that the ONI is a 3-month smoothed value, the monthly mean CWV anomaly is also smoothed in a 3-month moving window. Figure 3 depicts the ONI and monthly mean CWV anomalies from the radiosonde and reanalysis data. The CWV anomalies show a similar temporal evolution between the observation and the reanalysis with a significant correlation coefficient R=0.83, but tends to vary in opposite to the ONI but with a delay of about several months. The correlation coefficient between

https://doi.org/10.5194/acp-2021-345
Preprint. Discussion started: 29 April 2021

the CWV anomaly and the ONI is calculated to be -0.63 (-0.62) with a lag of 3 (2) months. One can note from Fig. 3 that when a strong La Niña occurs with ONI=-1.64 in November 2010, the water vapor anomaly reaches the positive maximum in February and March 2011 from the observation and reanalysis data, respectively. However, for the 2015/16 super El Niño event with the peak of ONI=2.6 in December 2015, an extremely negative anomaly appears in both the observation and reanalysis. The negative anomaly attains as large as -5.39 and -5.75 kg m^{-2} in February 2016 from the radiosonde and reanalysis data, respectively. Similarly, the 2009/10 event has a large index of ONI=1.6 in November 2009, which leads to the strong CWV anomalies of -2.45 and -3.94 kg m^{-2} in January 2010 from the radiosonde and reanalysis data, respectively. Hence, the ENSO or SST anomaly plays an important role in the water vapor variation in the tropical western Pacific.

4 Contribution from Tropical Circulations

4.1 Tropical Atmospheric Circulations

Besides the SST effect, evaporated sea water is carried to higher levels by the upward flow, thus the water vapor variability in the troposphere is closely related to the atmospheric circulation. In the tropics, there are several well-known circulations, i.e. Hadley, Walker and monsoon circulations, and each circulation has its own features and driving force though these circulations may be highly coupled with each other. In this way, we attempt to estimate the contributions of each tropical circulation to the observed water vapor anomalies in the El Niño events. According to the Helmholtz's theorem, horizontal wind velocity can be decomposed into the rotational and divergent winds,

$$\vec{V}_H = \vec{V}_\Psi + \vec{V}_\Phi = \vec{k} \times \nabla\Psi - \nabla\Phi \qquad (5)$$

where Ψ is the stream function, Φ is the velocity potential; $\vec{k}$ is the unit vector in the vertical

https://doi.org/10.5194/acp-2021-345
Preprint. Discussion started: 29 April 2021

direction; and $\vec{V}_H$, $\vec{V}_\Psi$ and $\vec{V}_\Phi$ are the horizontal, rotational and divergent wind velocities, respectively. Thermal driving force resulted from differential heating and temperature contrast is essential to cause atmospheric convergence-divergence and vertical motion and then the formation of atmospheric circulation. The stream function involved in the rotation field has no contribution to the atmospheric vertical motion, while the velocity potential may be chosen as the indicator of the atmospheric circulations since it is in connection with the atmospheric convergence-divergence associated with the upward and downward motions in the tropical region (Kanamitsu and Krishnamurti, 1978; Newell et al., 1996; Wang, 2002). Thus we selected the velocity potential at 850 hPa to represent the characteristics of the tropical circulations in the lower troposphere. The divergence and velocity potential fields are calculated by using the ECMWF reanalysis horizontal winds at 850 hPa according to the following equation (Krishnamurti, 1971; Tanaka et al., 2004),

$$D = \nabla \cdot \vec{V}_H = -\nabla^2 \Phi \tag{6}$$

where D is the divergence of horizontal wind. In Eq. (6), the negative sign means that the divergent wind flows from the large velocity potential to the small velocity potential.

Based on the different driving mechanisms and movement features, Tanaka et al. (2004) introduced the definitions of the Hadley, Walker and monsoon circulations, which have an advantage to quantitatively evaluate the intensity of the three tropical circulations by means of the separation of the velocity potential into three orthogonal spatial patterns. Thus, we follow the definitions and methodology proposed by Tanaka et al. (2004) to obtain these tropical circulations for investigating their contributions to the observed water vapor anomaly in the four El Niño events. The velocity potential is divided as (Tanaka et al., 2004),

$$\Phi(x,y,t) = [\Phi(t,y)] + \overline{\Phi^*}(x,y) + \Phi^{*\prime}(x,y,t) \tag{7}$$

https://doi.org/10.5194/acp-2021-345
Preprint. Discussion started: 29 April 2021

where x, y and t are the longitude, latitude and time, respectively. The square brackets and asterisk denote the zonal mean and the deviation from the zonal mean, respectively, and the overbar and prime denote the annual mean and the departure from the annual mean, respectively. The first term on the right of Eq. (7) is the zonal mean component of the velocity potential field, defined as the Hadley circulation because this circulation, driven by the large-scale meridional differential heating, may be treated as axisymmetric. The second and third terms on the right are the annual mean of the deviation from the zonal mean and the deviation from the annual mean, respectively. The third term is regarded to be the monsoon circulation since the monsoon circulation has the conspicuous seasonal variability as the sea-land heat contrast changes. The second term is referred to as the Walker circulation. The separation is not perfect for the Walker circulation without seasonal variation, as pointed out by Tanaka et al. (2004). The Walker circulation is induced by the different SST along the equator. Considering that the El Niño usually lasts for more than a year with the maximum ONI in winter, we chose the period of June to the next May to estimate the Walker circulation, and then obtain the Walker circulation anomaly during El Niño relative to its climatic average. In this way, the problem may not be very serious. The definitions and decomposition of the tropical circulations have extensively been used to study the influences of SST warming pattern on the interannual variation and long-term trend of the Hadley, Walker and monsoon circulations in association with hydrological cycle (Tanaka et al., 2005; Park and Sohn, 2008; Li and Feng, 2013; Ma and Xie, 2013).

According to Eq. (6), we calculate the time series of the divergent wind and velocity potential at 850 hPa from 2005 to 2019 by using the reanalysis horizontal wind data, and then their monthly climatic normal is derived from their time series, respectively. Figure 4 presents the climatic means of the velocity potential and divergent wind fields in DJF. We choose the velocity potential as the proxy of the circulation intensity, thus the intensity of the tropical circulation in winter can clearly be seen from Fig. 4. The prominent negative peak of about -90 $\times 10^5$ m^2 s^{-1} in the velocity potential is situated in the western Pacific warm pool, thus there is the convergence center of horizontal wind field, which induces the rising motion in the lower troposphere over the region, including the five radiosonde stations. Hence, the atmospheric water vapor is abundant in this region due to the transportation by the strong ascending flow. On the contrary, the maximum (second) velocity potential of 44×10^5 (42×10^5) m^2 s^{-1} appears in the southeast Pacific (Indian) ocean, meaning the divergence center and the sinking motion over there, as well as less water vapor relative to the western Pacific warm pool region.

4.2 Atmospheric Circulation Anomalies

Next, we focus on the tropical circulation anomaly in the four El Niño events. Figure 5 illustrates the velocity potential and divergent wind anomalies at 850 hPa in the four winters. Here, we define the velocity potential value as the circulation index with the units measured by 10^5 m^2 s^{-1}, and accordingly, the velocity potential anomaly is regarded as the index of the circulation anomaly. As a consequence, the positive index of the circulation anomaly indicates the weakened convergence and rising motion or the strengthened divergence and sinking motion, and vice versa for the negative index of the circulation anomaly. Hence, the positive and negative indices mean the decrease and increase of water vapor in the troposphere due to the vertical transport change, respectively. In Fig. 5, the positive index of the circulation anomaly occurs in the western Pacific, especially in the 2009/10 and 2015/16 El Niño winters, thus the ascending motion is suppressed over there, and the negative water vapor anomalies are recorded in the radiosonde observation. On the contrary, there is the negative index in the equatorial eastern Pacific, which causes that the descending flow is suppressed. Correspondingly, the positive CWV anomaly over the equatorial eastern Pacific can be seen from Fig. 2.

https://doi.org/10.5194/acp-2021-345
Preprint. Discussion started: 29 April 2021

According to Eq. (7), we calculate the velocity potential of the Hadley, Walker and monsoon circulations and their anomaly indices at 850 hPa from the reanalysis data. Figure 6 presents the velocity potential and anomaly index of the Hadley circulation in the four El Niño winters. Now that the Hadley circulation is a tropical circulation driven by the meridional differential heating in the global radiative process (Oort and Yienger, 1996), this large-scale circulation is very similar in different winters with the circulation index increasing from the negative peak at about 12°S to positive peak at 23°N, and is little affected by El Niño with the anomaly index less than 2×10^5 $m^2 s^{-1}$, or 2 units. Even so, the pattern of the Hadley circulation anomaly is distinguished between the EP El Niño and CP El Niño. During the CP El Niño winters, the index of the Hadley circulation anomaly is positive over the entire tropics with the maximum of 1.74 (1.65) units at 3°N (2°N) in the 2018/19 (2009/10) winter. Whereas, in the 2006/07 and 2015/16 EP El Niño winters, the positive index is located at about 5°N-30°N, and the negative index occurs over about 30°S-5°N. At the five radiosonde sites, the averaged anomaly index is 0.29, 1.56, 0.65 and 1.37 units in the 2006/07, 2009/10, 2015/06 and 2018/19 winters, respectively, indicating that the Hadley circulation is too stable to have a significant impact on the water vapor variation.

Figure 7 depicts the velocity potential and anomaly index of the Walker circulation at 850 hPa in the El Niño winters. Relative to the Hadley circulation, the Walker circulation is the local circulation formed over the tropical Pacific with intense ascending flow in the western Pacific and descending flow in the eastern Pacific, thus the circulation has a high variability with the SST anomaly caused by ocean current. As the Walker circulation is directly related to ENSO, the scenario of the Walker circulation anomalies is roughly consistent with each other among the four El Niño events. In general, the positive and negative indices of the Walker circulation anomaly are located in the western and eastern Pacific, opposite to the circulation index, respectively, which illustrates that the Walker circulation anomaly in El Niño

https://doi.org/10.5194/acp-2021-345
Preprint. Discussion started: 29 April 2021

Atmospheric Chemistry and Physics Discussions

suppresses the strong rising in the western Pacific and sinking in the eastern Pacific. Nevertheless, the strength of the circulation anomaly is the significant difference among the four events. In the 2015/16 winter, the Walker circulation anomaly, with the peak indices as large as 26.8 and -27.7 units in the equatorial Pacific, are much stronger than in the other three winters. Hence, the Walker circulation variation plays a key role in the CWV anomaly during the 2015/16 supper El Niño event.

The velocity potential and anomaly index of the monsoon circulation in the four El Niño winters are plotted in Fig. 8. The monsoon circulation in the lower atmosphere blows from the land to the sea in winter, thus it can be seen from Fig. 8 that the pattern of the monsoon circulation is evidently different from that of the Walker circulation shown in Fig. 7. The anomaly of the monsoon circulation is sensitive to the type of El Niño, which is also distinguished from that of the Walker circulation. Early studies showed that the CP and EP El Niños have different effects on the Indian and eastern Asian monsoon rainfall (Weng et al., 2008; Wang et al., 2013). The monsoon circulation anomaly in the radiosonde stations has the index around zero in the EP El Niño events, which is far weaker relative to the large positive index in the CP El Niño events, similar to previous investigation (Fan et al, 2017). In the 2009/10 El Niño event, the pronounced anomaly with the peak index of 17.8 units takes place in the western Pacific, which implies that the monsoon circulation anomaly has an important influenced on the negative water vapor anomaly in the radiosonde observation.

4.3 Contribution to Water Vapor Anomaly

We estimate the contributions of the Hadley, Walker and monsoon circulation anomalies to the water vapor anomaly observed by the radiosonde in the four El Niño events by means of comparing the indices of the circulation anomalies. Figure 9 illustrates the indices of the circulation anomalies at 850 hPa and the CWV anomalies derived from the radiosonde and reanalysis data, and these circulation

https://doi.org/10.5194/acp-2021-345
Preprint. Discussion started: 29 April 2021

anomaly indices and CWV anomalies are the values averaged at the five radiosonde sites in winter. Although there is some difference in the intensity of the CWV anomaly between the reanalysis and radiosonde data, both of them increase with the increasing index of the total circulation anomaly. As discussed above, the contribution of the Hadley circulation anomaly is very small with the maximum of only 1.56 units in the 2009/10 event. The anomaly of the Walker circulation makes a considerable contribution in each case, especially for the EP El Niño events, it is the strongest in the three tropical circulation anomalies. The index of the Walker circulation anomaly counts for 92.3% of the total anomaly index (23.89 units) in the 2015/16 El Niño winter, and even exceeds the total index in the 2006/07 event owing to the negative anomaly of the monsoon circulation. The anomaly of the monsoon circulation shows an evident change from one to the other event because it is sensitive to the local heat contrast and the El Niño shift. In the western Pacific, the CP El Niño can lead to the obvious positive anomaly of the monsoon circulation. The index of the monsoon circulation anomaly is about 69.7% (44.7%) of the total anomaly index in the 2009/10 (2018/19) CP El Niño winter. Consequently, for the two intense El Niño events, the water vapor anomaly is caused mainly by the Walker circulation anomaly in the 2015/16 EP event but by the monsoon circulation anomaly in the 2009/10 CP event, respectively. The Walker and monsoon circulation anomalies nearly equally (oppositely) contribute to the CWV anomaly in the 2018/19 (2006/07) event. Therefore, the Hadley, Walker and monsoon circulation anomalies may have the remarkable differences in the contributions to the water vapor variation in different El Niño events.

In the 2015/16 and 2018/19 winters, the reanalysis CWV anomalies of -4.34 and -1.30 kg m^{-2} are roughly consistent with -4.46 and -1.54 kg m^{-2} in the radiosonde observation, respectively. However, in the first two events, there is a distinct difference between the reanalysis and radiosonde data. At least in

Atmospheric Chemistry and Physics Discussions

the 2009/10 winter, we speculate that the reanalysis data may underestimate the tropospheric water vapor over the five stations, which can further be confirmed by the changes in the cloud and OLR data.

5 Changes in Cloud and OLR

Using the cloud occurrence from the CALIPSO during June 2006 to December 2016, we calculate tropical cloud fraction between 0°N and 15°N in the 2006/07, 2009/10 and 2015/16 winters and its climatic mean in winter, which is shown in Fig. 10. We also compute the OLR anomalies over 30°S-30°N in the four El Niño winters based on the monthly OLR data between 2005 and 2019. Figure 11 shows the OLR anomalies in the four El Niño events. In the western Pacific, the strong rising flow carries abundant water vapor to high level due to the convergence of horizontal wind field in winter, as shown in Fig. 4, and then the water vapor condenses to form clouds as it cools, thus there is cloudy over the tropical western Pacific. In the El Niño events, the cloud amount decreases from about 80°E to 160°E but tends to increase between about 160°E to 120°W because of the tropical circulation changes. Owing to the reflection effect of cloud on OLR, the OLR change is opposite to the variation of cloud amount. In the 2009/10 and 2015/16 strong El Niño winters, the OLR is obviously enhanced in the tropical northwest Pacific and significantly reduced in the equatorial mid-eastern Pacific as the cloud occurrence changes. Hence, the cloud and OLR have a clear response to the water vapor anomaly in the El Niño events.

As described above, the reanalysis CWV anomaly at the radiosonde stations in the 2009/10 winter has an almost same intensity as that in the 2015/16 winter, but the radiosonde observation indicates that the water vapor reduction is evidently less in the 2009/10 winter than in the 2015/16 winter. As shown in Figs. 10 and 11, the satellite observation shows that there exist less cloud occurrence and more OLR at

https://doi.org/10.5194/acp-2021-345
Preprint. Discussion started: 29 April 2021

the radiosonde stations in the 2015/16 winter compared with in the 2009/10 winter. Therefore, this supports the radiosonde observation and our suggestion that the reanalysis data underestimates the tropospheric water vapor over the radiosonde stations in the 2009/10 winter.

6 Summary

In the paper, we report the significantly negative water vapor anomaly in the troposphere during the four El Niño winters at the five radiosonde stations in the tropical western Pacific based on the radiosonde and reanalysis data for 15 years from 2005 to 2019, and study the relationship between the water vapor anomaly and the El Niño index and the contribution of the different tropical circulation anomalies to the observed water vapor anomaly in the El Niño events.

The radiosonde observation shows that the negative water vapor anomaly arises in the El Niño winters, in particular, an extremely negative anomaly in the 2015/16 supper El Niño event. The prominent specific humidity anomaly is concentrated below 8 km of the troposphere with the peak at the height of about 2.5-3.5 km. The local CWV anomaly has a large negative correlation coefficient of -0.63 with the ONI in the Niño3.4 region, but with a lag of about 2-3 months. The reanalysis data reveals that the negative water vapor anomaly widely occurs in the tropical northwest Pacific, while correspondingly, the positive anomaly takes place in the equatorial mid-eastern Pacific. The 2015/16 El Niño event, with ONI=2.6, is the strongest during the 15 years, leading to the extreme anomaly in the water vapor over the tropical Pacific.

The atmospheric water vapor from tropical sea water evaporation is affected not only by the SST, but also by the vertical motion of the atmosphere which can transport the water vapor from the near-sea surface to the high level. By using the definitions and method introduced by Tanaka et al. (2004), we decompose the tropical circulation into the Hadley, Walker and monsoon circulations to estimate their contributions to the observed water vapor anomaly in the four El Niño events. In general, the tropical circulation anomaly in the El Niño winter is characterized by divergence (convergence) at 850 hPa in the tropical western (eastern) Pacific, thus the CWV decreases over the tropical western Pacific as the ascending flow is suppressed. As the large-scale meridional circulation driven by the differential heating, the variation of the Hadley circulation is pretty small with the anomaly index less than 2 units. At the radiosonde stations, the anomaly of the Walker circulation makes a considerable contribution to the total anomaly in all the El Niño winters, especially in the 2006/07 and 2015/16 EP El Niño event. The monsoon circulation exhibits an obvious variability from one to the other event, and its anomaly is large in the 2009/10 and 2018/19 CP El Niño winters and small in the 2006/07 and 2015/16 EP El Niño winters. Therefore, the observed water vapor anomaly is caused mainly by the Walker circulation anomaly in the 2015/16 supper EP event but by the monsoon circulation anomaly in the 2009/10 strong CP event, respectively.

Because of the reduction in the upward transport of water vapor over the tropical western Pacific in the El Niño events, the satellite observation shows that relative to the climatic means, the cloud decreases, and the OLR is accordingly strengthened, in particular, during the strong El Niño winters of 2009/10 and 2015/16. In addition, both the radiosonde and satellite observations suggest that the tropospheric water vapor over the region is underestimated in the reanalysis data during the 2009/10 winter.

Data availability. The radiosonde observation is provided by the NOAA at the website of ftp://ftp.ncdc.noaa.gov/pub/data/ua/rrs-data/. The ERA5 reanalysis data is from the ECMWF at https://cds.climate.copernicus.eu/cdsapp#!/home/. The Niño3.4 index is from the NOAA at https://catalog.data.gov/dataset/climate-prediction-center-cpcoceanic-nino-index/. The OLR data is from the NOAA at https://www.esrl.noaa.gov/psd/data/gridded/data.interp_OLR.html/. The cloud occurrence monthly data is from the NASA at https://eosweb.larc.nasa.gov/project/calipso/cloud_occurrence_table/.

Author contributions. KH and MD proposed the scientific ideas. MD and KH completed the analysis and the manuscript. SZ, CH, YG and FY discussed the results in the manuscript.

Competing interests. The authors declare that they have no conflict of interest.

Acknowledgments. This work was supported by the National Natural Science Foundation of China (through grants 41974176).

References

Ashok, K., Behera, S. K., Rao, S. A., Weng, H., and Yamagata, T.: El Niño Modoki and its possible teleconnection, J. Geophys. Res., 112, https://doi.org/10.1029/2006jc003798, 2007.

Avery, M. A., Davis, S. M., Rosenlof, K. H., Ye, H., and Dessler, A. E.: Large anomalies in lower stratospheric water vapour and ice during the 2015–2016 El Niño, Nat. Geosci., 10, 405-409, https://doi.org/10.1038/ngeo2961, 2017.

Dai, A. and Wigley, T. M. L.: Global patterns of ENSO-induced precipitation, Geophys. Res. Lett., 27, 1283-1286, https://doi.org/10.1029/1999gl011140, 2000.

Dunkerton, T. J.: The quasi-biennial oscillation of 2015-2016: Hiccup or death spiral?, Geophys. Res. Lett.,

https://doi.org/10.5194/acp-2021-345
Preprint. Discussion started: 29 April 2021

43, 10,547-510,552, https://doi.org/10.1002/2016gl070921, 2016.

Fan, F., Dong, X., Fang, X., Xue, F., Zheng, F., and Zhu, J.: Revisiting the relationship between the South Asian summer monsoon drought and El Niño warming pattern, Atmos. Sci. Let., 18, 175-182, https://doi.org/10.1002/asl.740, 2017.

Gasparin, F. and Roemmich, D.: The strong freshwater anomaly during the onset of the 2015/2016 El Niño, Geophys. Res. Lett., 43, 6452-6460, https://doi.org/10.1002/2016gl069542, 2016.

Gu, G. and Adler, R. F.: Precipitation, temperature, and moisture transport variations associated with two distinct ENSO flavors during 1979–2014, Climate Dyn., 52, 7249-7265, https://doi.org/10.1007/s00382-016-3462-3, 2016.

Held, I. M. and Soden, B. J.: Water Vapor Feedback and Global Warming, Annu. Rev. Energy Env., 25, 441-475, https://doi.org/10.1146/annurev.energy.25.1.441, 2000.

Hersbach, H., Bell, B., Berrisford, P., Hirahara, S., Horányi, A., Muñoz‐Sabater, J., Nicolas, J., Peubey, C., Radu, R., Schepers, D., Simmons, A., Soci, C., Abdalla, S., Abellan, X., Balsamo, G., Bechtold, P., Biavati, G., Bidlot, J., Bonavita, M., Chiara, G., Dahlgren, P., Dee, D., Diamantakis, M., Dragani, R., Flemming, J., Forbes, R., Fuentes, M., Geer, A., Haimberger, L., Healy, S., Hogan, R. J., Hólm, E., Janisková, M., Keeley, S., Laloyaux, P., Lopez, P., Lupu, C., Radnoti, G., Rosnay, P., Rozum, I., Vamborg, F., Villaume, S., and Thépaut, J. N.: The ERA5 global reanalysis, Q. J. R. Meteorol. Soc., 146, 1999-2049, https://doi.org/10.1002/qj.3803, 2020.

Hill, K. J., Taschetto, A. S., and England, M. H.: South American rainfall impacts associated with inter-El Niño variations, Geophys. Res. Lett., 36, https://doi.org/10.1029/2009gl040164, 2009.

Huang, B. Y., Thorne, P. W., Banzon, V. F., Boyer, T., Chepurin, G., Lawrimore, J. H., Menne, M. J., Smith, T. M., Vose, R. S., and Zhang, H. M.: Extended Reconstructed Sea Surface Temperature, Version 5

https://doi.org/10.5194/acp-2021-345
Preprint. Discussion started: 29 April 2021

(ERSSTv5): Upgrades, Validations, and Intercomparisons, J. Climate, 30, 8179-8205, https://doi.org/10.1175/jcli-d-16-0836.1, 2017.

Ishida, A., Kashino, Y., Hosoda, S., and Ando, K.: North-south asymmetry of warm water volume transport related with El Niño variability, Geophys. Res. Lett., 35, https://doi.org/10.1029/2008gl034858, 2008.

Kanamitsu, M. and Krishnamurti, T. N.: Northern Summer Tropical Circulations During Drought and Normal Rainfall Months, Mon. Weather Rev., 106, 331-347, https://doi.org/10.1175/1520-0493(1978)106<0331:Nstcdd>2.0.Co;2, 1978.

Krishnamurti, T. N.: Tropical East-West Circulations During the Northern Summer, J. Atmos. Sci., 28, 1342-1347, https://doi.org/10.1175/1520-0469(1971)028<1342:TEWCDT>2.0.CO;2, 1971.

Kug, J.-S., Jin, F.-F., and An, S.-I.: Two Types of El Niño Events: Cold Tongue El Niño and Warm Pool El Niño, J. Climate, 22, 1499-1515, https://doi.org/10.1175/2008JCLI2624.1, 2009.

L'Heureux, M. L., Takahashi, K., Watkins, A. B., Barnston, A. G., Becker, E. J., Di Liberto, T. E., Gamble, F., Gottschalck, J., Halpert, M. S., Huang, B., Mosquera-Vásquez, K., and Wittenberg, A. T.: Observing and Predicting the 2015/16 El Niño, Bull. Amer. Meteor. Soc., 98, 1363-1382, https://doi.org/10.1175/bams-d-16-0009.1, 2017.

Lanzante, J. R.: RESISTANT, ROBUST AND NON-PARAMETRIC TECHNIQUES FOR THE ANALYSIS OF CLIMATE DATA: THEORY AND EXAMPLES, INCLUDING APPLICATIONS TO HISTORICAL RADIOSONDE STATION DATA, Int. J. Climatol., 16, 1197-1226, https://doi.org/10.1002/(SICI)1097-0088(199611)16:11<1197::AID-JOC89>3.0.CO;2-L, 1996.

Lee, S.-K., Mapes, B. E., Wang, C., Enfield, D. B., and Weaver, S. J.: Springtime ENSO phase evolution and its relation to rainfall in the continental U.S, Geophys. Res. Lett., 41, 1673-1680,

https://doi.org/10.5194/acp-2021-345
Preprint. Discussion started: 29 April 2021

https://doi.org/10.1002/2013gl059137, 2014.

Li, J. and Feng, J.: Contrasting Impacts of Two Types of ENSO on the Boreal Spring Hadley Circulation, J. Climate, 26, 4773-4789, https://doi.org/10.1175/jcli-d-12-00298.1, 2013.

Li, Z., Li, Y., Bonsal, B., Manson, A. H., and Scaff, L.: Combined impacts of ENSO and MJO on the 2015 growing season drought on the Canadian Prairies, Hydrol. Earth Syst. Sci., 22, 5057-5067, https://doi.org/10.5194/hess-22-5057-2018, 2018.

Liebmann, B. and Smith, C. A.: Description of a Complete (Interpolated) Outgoing Longwave Radiation Dataset, Bull. Amer. Meteor. Soc., 77, 1275-1277, 1996.

López-Parages, J. and Rodríguez-Fonseca, B.: Multidecadal modulation of El Niño influence on the Euro-Mediterranean rainfall, Geophys. Res. Lett., 39, https://doi.org/https://doi.org/10.1029/2011GL050049, 2012.

Ma, J. and Xie, S.-P.: Regional Patterns of Sea Surface Temperature Change: A Source of Uncertainty in Future Projections of Precipitation and Atmospheric Circulation, J. Climate, 26, 2482-2501, https://doi.org/10.1175/jcli-d-12-00283.1, 2013.

Madenach, N., Carbajal Henken, C., Preusker, R., Sourdeval, O., and Fischer, J.: Analysis and quantification of ENSO-linked changes in the tropical Atlantic cloud vertical distribution using 14 years of MODIS observations, Atmos. Chem. Phys., 19, 13535-13546, https://doi.org/10.5194/acp-19-13535-2019, 2019.

Mapes, B., Chandra, A. S., Kuang, Z., and Zuidema, P.: Importance Profiles for Water Vapor, Surv. Geophys., 38, 1355-1369, https://doi.org/10.1007/s10712-017-9427-1, 2017.

Mariotti, A.: How ENSO impacts precipitation in southwest central Asia, Geophys. Res. Lett., 34, https://doi.org/10.1029/2007gl030078, 2007.

https://doi.org/10.5194/acp-2021-345
Preprint. Discussion started: 29 April 2021

Massie, S., Lowe, P., Tie, X., Hervig, M., Thomas, G., and Russell, J.: Effect of the 1997 El Niño on the distribution of upper tropospheric cirrus, J. Geophys. Res.-Atmos., 105, 22725-22741, https://doi.org/10.1029/2000jd900322, 2000.

Murray, F. W.: On the Computation of Saturation Vapor Pressure, J. Appl, Meteorol., 6, 203-204, https://doi.org/10.1175/1520-0450(1967)006<0203:OTCOSV>2.0.CO;2 1967.

Newell, R. E., Zhu, Y., Browell, E. V., Read, W. G., and Waters, J. W.: Walker circulation and tropical upper tropospheric water vapor, J. Geophys. Res.-Atmos., 101, 1961-1974, https://doi.org/10.1029/95jd02275, 1996.

Newman, P. A., Coy, L., Pawson, S., and Lait, L. R.: The anomalous change in the QBO in 2015-2016, Geophys. Res. Lett., 43, 8791-8797, https://doi.org/10.1002/2016gl070373, 2016.

Okazaki, A., Satoh, Y., Tremoy, G., Vimeux, F., Scheepmaker, R., and Yoshimura, K.: Interannual variability of isotopic composition in water vapor over western Africa and its relationship to ENSO, Atmos. Chem. Phys., 15, 3193-3204, https://doi.org/10.5194/acp-15-3193-2015, 2015.

Oort, A. H. and Yienger, J. J.: Observed Interannual Variability in the Hadley Circulation and Its Connection to ENSO, J. Climate, 9, 2751-2767, https://doi.org/10.1175/1520-0442(1996)009<2751:OIVITH>2.0.CO;2, 1996.

Paek, H., Yu, J.-Y., and Qian, C.: Why were the 2015/2016 and 1997/1998 extreme El Niños different?, Geophys. Res. Lett., https://doi.org/10.1002/2016gl071515, 2017.

Palmeiro, F. M., Iza, M., Barriopedro, D., Calvo, N., and García-Herrera, R.: The complex behavior of El Niño winter 2015-2016, Geophys. Res. Lett., 44, 2902-2910, https://doi.org/10.1002/2017gl072920, 2017.

Park, S.-C. and Sohn, B.-J.: Recent trend of Hadley and Walker circulation shown in water vapor transport

https://doi.org/10.5194/acp-2021-345
Preprint. Discussion started: 29 April 2021

potential, in: 20th Conference on Climate Variability and Change, General Climate Studies: Poster Session, New York, United States, 21 January 2008, P2.18, 2008.

Permana, D. S., Thompson, L. G., and Setyadi, G.: Tropical West Pacific moisture dynamics and climate controls on rainfall isotopic ratios in southern Papua, Indonesia, J. Geophys. Res.-Atmos., 121, 2222-2245, https://doi.org/10.1002/2015jd023893, 2016.

Quartly, G. D., Srokosz, M. A., and Guymer, T. H.: Changes in oceanic precipitation during the 1997-98 El Niño, Geophys. Res. Lett., 27, 2293-2296, https://doi.org/10.1029/1999gl011311, 2000.

Sandeep, S. and Ajayamohan, R. S.: Modulation of Winter Precipitation Dynamics Over the Arabian Gulf by ENSO, J. Geophys. Res.-Atmos., 123, 198-210, https://doi.org/10.1002/2017jd027263, 2018.

Soden, B. J., Held, I. M., Colman, R., Shell, K. M., Kiehl, J. T., and Shields, C. A.: Quantifying Climate Feedbacks Using Radiative Kernels, J. Climate, 21, 3504-3520, https://doi.org/10.1175/2007jcli2110.1, 2008.

Stevens, B., Brogniez, H., Kiemle, C., Lacour, J.-L., Crevoisier, C., and Kiliani, J.: Structure and Dynamical Influence of Water Vapor in the Lower Tropical Troposphere, Surv. Geophys., 38, 1371-1397, https://doi.org/10.1007/s10712-017-9420-8, 2017.

Su, H. and Jiang, J. H.: Tropical Clouds and Circulation Changes during the 2006/07 and 2009/10 El Niños, J. Climate, 26, 399-413, https://doi.org/10.1175/JCLI-D-12-00152.1, 2013.

Sun, M., Cess, R. D., and Doelling, D. R.: Interpretation of cloud structure anomalies over the tropical Pacific during the 1997/98 El Niño, J. Geophys. Res.-Atmos., 117, https://doi.org/10.1029/2011JD015861, 2012.

Takahashi, H., Su, H., Jiang, J. H., Luo, Z. J., Xie, S.-P., and Hafner, J.: Tropical water vapor variations during the 2006-2007 and 2009-2010 El Niños: Satellite observation and GFDL AM2.1 simulation, J.

Geophys. Res.-Atmos., 118, 8910-8920, https://doi.org/10.1002/jgrd.50684, 2013.

Tanaka, H. L., Ishizaki, N., and Kitoh, A.: Trend and interannual variability of Walker, monsoon and Hadley circulations defined by velocity potential in the upper troposphere, Tellus A, 56, 250-269, https://doi.org/10.1111/j.1600-0870.2004.00049.x, 2004.

Tanaka, H. L., Ishizaki, N., and Nohara, D.: Intercomparison of the Intensities and Trends of Hadley, Walker and Monsoon Circulations in the Global Warming Projections, SOLA, 1, 77-80, https://doi.org/10.2151/sola.2005-021, 2005.

Viswanadham, Y.: The Relationship between Total Precipitable Water and Surface Dew Point, J. Appl. Meteorol. Climatol., 20, 3-8, https://doi.org/10.1175/1520-0450(1981)020<0003:TRBTPW>2.0.CO;2, 1981.

Wang, C.: Atmospheric Circulation Cells Associated with the El Niño Southern Oscillation, J. Climate, 15, 399-419, https://doi.org/10.1175/1520-0442(2002)015<0399:ACCAWT>2.0.CO;2, 2002.

Wang, J., Zeng, N., Wang, M., Jiang, F., Chen, J., Friedlingstein, P., Jain, A. K., Jiang, Z., Ju, W., Lienert, S., Nabel, J., Sitch, S., Viovy, N., Wang, H., and Wiltshire, A. J.: Contrasting interannual atmospheric CO_2 variabilities and their terrestrial mechanisms for two types of El Niños, Atmos. Chem. Phys., 18, 10333-10345, https://doi.org/10.5194/acp-18-10333-2018, 2018.

Wang, X., Jiang, X., Yang, S., and Li, Y.: Different impacts of the two types of El Niño on Asian summer monsoon onset, Environ. Res. Lett., 8, https://doi.org/10.1088/1748-9326/8/4/044053, 2013.

Weng, H., Behera, S. K., and Yamagata, T.: Anomalous winter climate conditions in the Pacific rim during recent El Niño Modoki and El Niño events, Climate Dyn., 32, 663-674, https://doi.org/10.1007/s00382-008-0394-6, 2008.

Winker, D. M., Hunt, W. H., and McGill, M. J.: Initial performance assessment of CALIOP, Geophys. Res.

https://doi.org/10.5194/acp-2021-345
Preprint. Discussion started: 29 April 2021

Lett., 34, https://doi.org/10.1029/2007gl030135, 2007.

Xu, K., Tam, C.-Y., Zhu, C., Liu, B., and Wang, W.: CMIP5 Projections of Two Types of El Niño and Their Related Tropical Precipitation in the Twenty-First Century, J. Climate, 30, 849-864, https://doi.org/10.1175/jcli-d-16-0413.1, 2017.

Yan, X., Konopka, P., Ploeger, F., Tao, M., Müller, R., Santee, M. L., Bian, J., and Riese, M.: El Niño Southern Oscillation influence on the Asian summer monsoon anticyclone, Atmos. Chem. Phys., 18, 8079-8096, https://doi.org/10.5194/acp-18-8079-2018, 2018.

Yeh, S.-W., Kug, J.-S., Dewitte, B., Kwon, M.-H., Kirtman, B. P., and Jin, F.-F.: El Nino in a changing climate, Nature, 461, 511-514, https://doi.org/10.1038/nature08316, 2009.

Yeh, S.-W., Kug, J.-S., and An, S.-I.: Recent progress on two types of El Niño: Observations, dynamics, and future changes, Asia-Pac. J. Atmos. Sci., 50, 69-81, https://doi.org/10.1007/s13143-014-0028-3, 2014.

Yu, J.-Y. and Kao, H.-Y.: Contrasting Eastern-Pacific and Central-Pacific Types of ENSO, J. Climate, 22, 615-632, https://doi.org/10.1175/2008jcli2309.1, 2009.

Zhao, P., Yang, S., and Yu, R.: Long-Term Changes in Rainfall over Eastern China and Large-Scale Atmospheric Circulation Associated with Recent Global Warming, J. Climate, 23, 1544-1562, https://doi.org/10.1175/2009jcli2660.1, 2010.

https://doi.org/10.5194/acp-2021-345
Preprint. Discussion started: 29 April 2021

Atmospheric Chemistry and Physics
Discussions

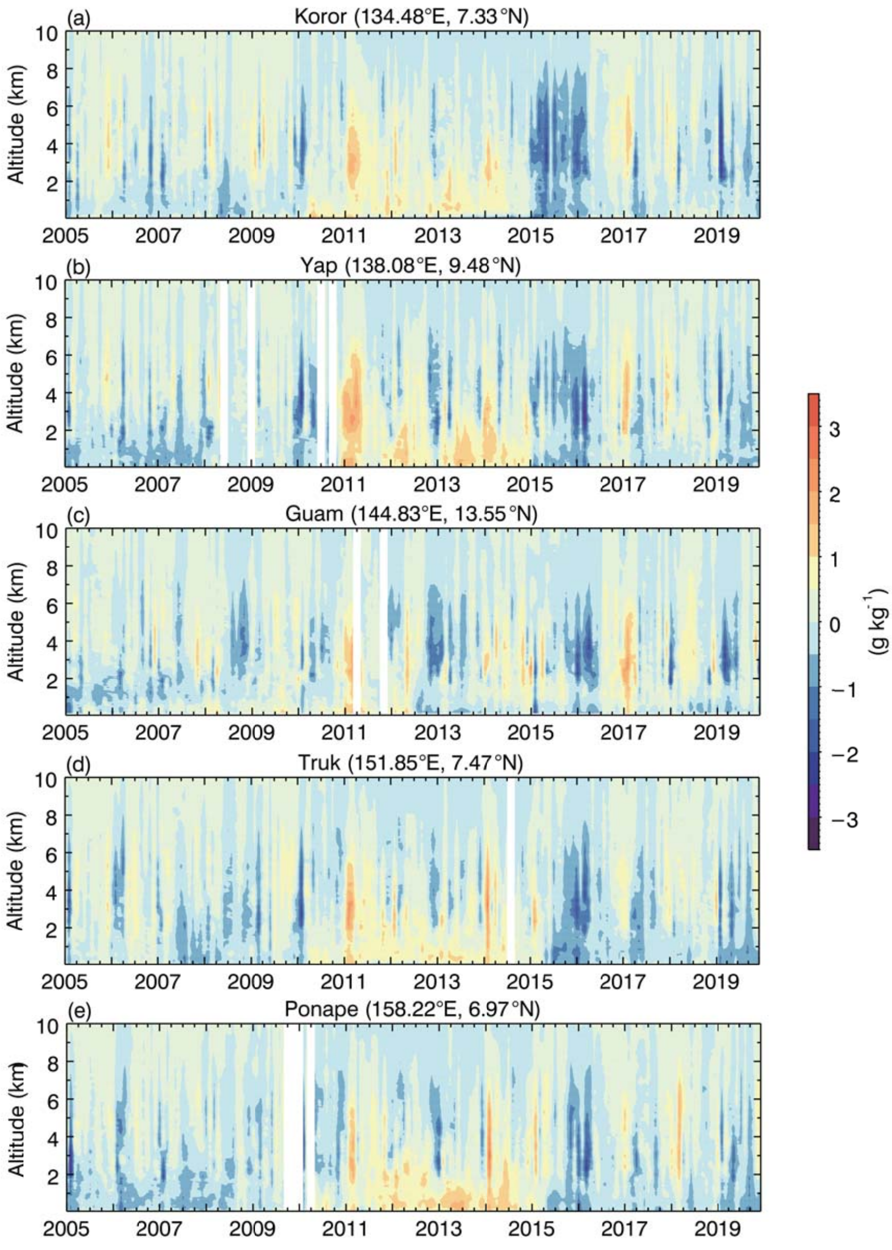

589

590 **Figure 1.** Specific humidity anomaly between January 2005 and December 2019 derived from radiosonde

591 observations at (a) Koror, (b) Yap, (c) Guam, (d) Truk and (e) Ponape.

https://doi.org/10.5194/acp-2021-345
Preprint. Discussion started: 29 April 2021

Atmospheric Chemistry and Physics
Open Access
Discussions

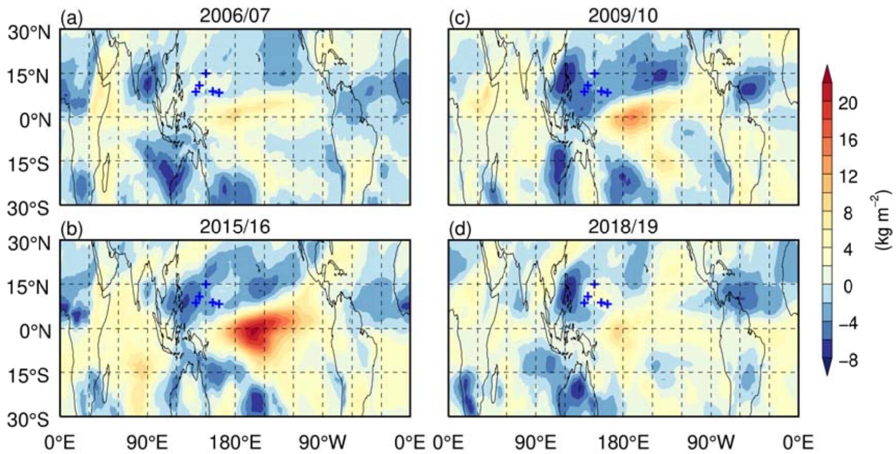

Figure 2. CWV anomalies averaged in (a) 2006/07, (b) 2015/16, (c) 2009/10 and (d) 2018/19 winters derived from ECMWF reanalysis data. The blue plus denotes the five radiosonde stations. The four El Niño events are classified into (left) EP El Niño and (right) CP El Niño.

https://doi.org/10.5194/acp-2021-345
Preprint. Discussion started: 29 April 2021

Atmospheric Chemistry and Physics
Discussions

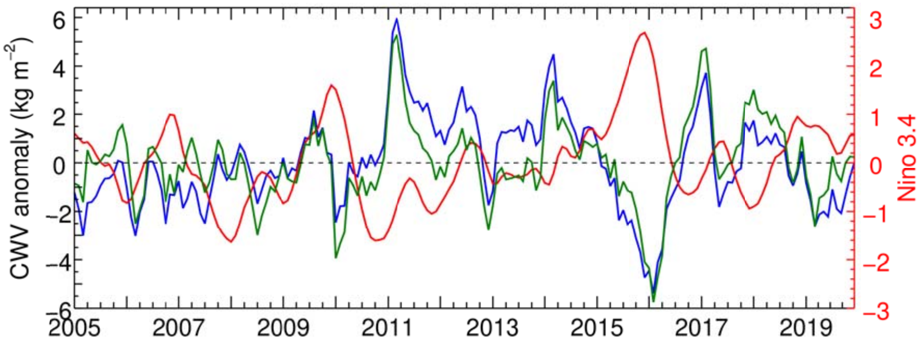

Figure 3. Time series of (red) ONI index and monthly mean CWV anomalies derived from (blue) radiosonde observation and (green) reanalysis data at five radiosonde stations.

Atmospheric Chemistry and Physics
Discussions

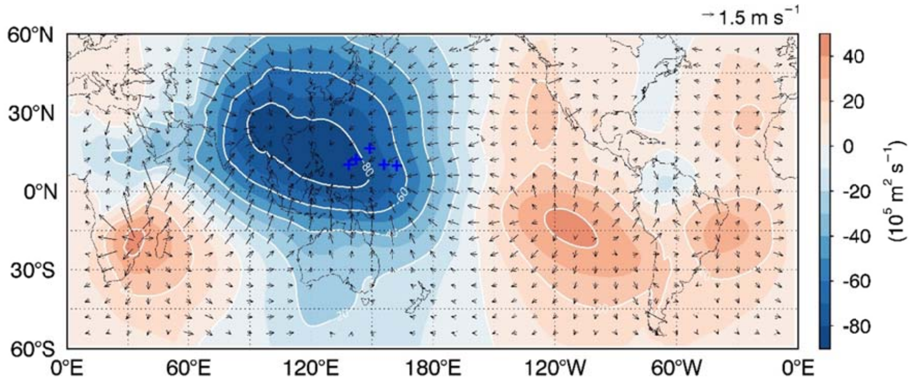

Figure 4. Climatic means of (shading) velocity potential and (arrow) divergent wind fields at 850 hPa in DJF derived from reanalysis data during 2005-2019. The blue plus denotes the five radiosonde stations.

https://doi.org/10.5194/acp-2021-345
Preprint. Discussion started: 29 April 2021

Atmospheric Chemistry and Physics
Discussions

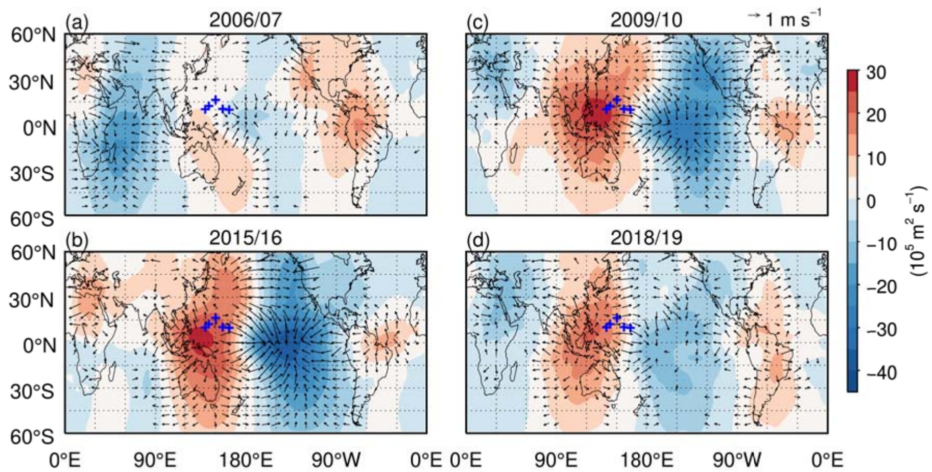

Figure 5. Anomalies of (shading) velocity potential and (arrow) divergent wind at 850 hPa in winters of (a) 2006/07, (b) 2015/16, (c) 2009/10 and (d) 2018/19. The blue plus denotes the five radiosonde stations.

https://doi.org/10.5194/acp-2021-345
Preprint. Discussion started: 29 April 2021

Atmospheric Chemistry and Physics
Discussions

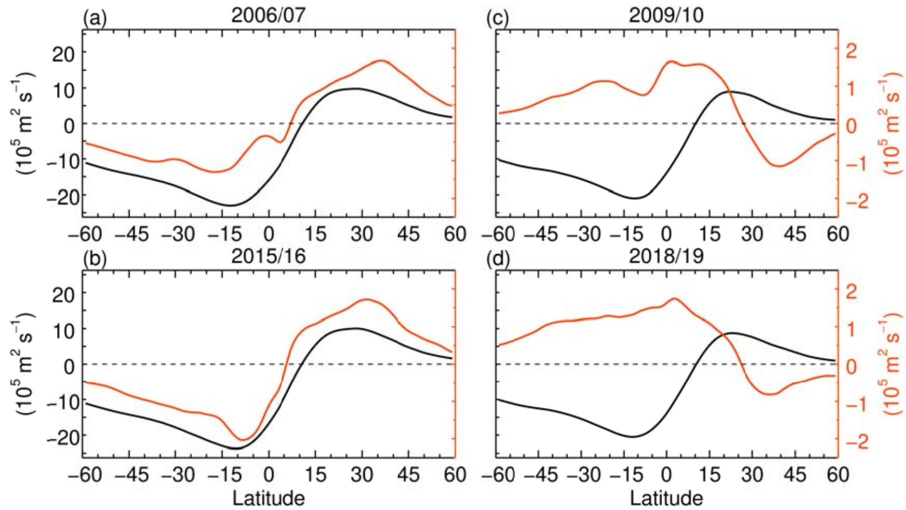

Figure 6. (Black)Velocity potential and (orange) anomaly index of Hadley circulation at 850 hPa in (a) 2006/07, (b) 2015/16, (c) 2009/10 and (d) 2018/19 winters.

https://doi.org/10.5194/acp-2021-345
Preprint. Discussion started: 29 April 2021

Atmospheric Chemistry and Physics
Discussions

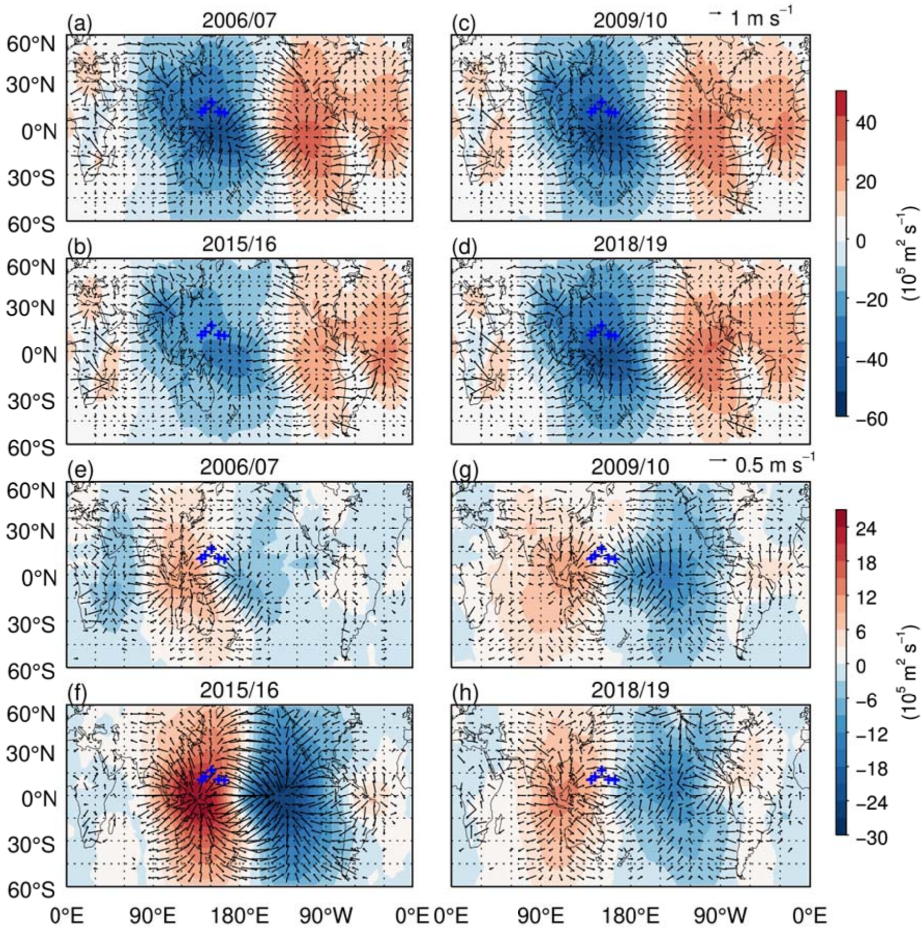

Figure 7. (shading) Velocity potential and (arrow) divergent wind of Walker circulation and their anomalies at 850 hPa in (a, e) 2006/07, (b, f) 2015/16, (c, g) 2009/10 and (d, h) 2018/19 winters. Figure 7(a-d) denotes the velocity potential and divergent wind, and Figure 7(e-h) denotes their anomalies. The blue plus denotes the five radiosonde stations.

https://doi.org/10.5194/acp-2021-345
Preprint. Discussion started: 29 April 2021

Atmospheric Chemistry and Physics
Discussions

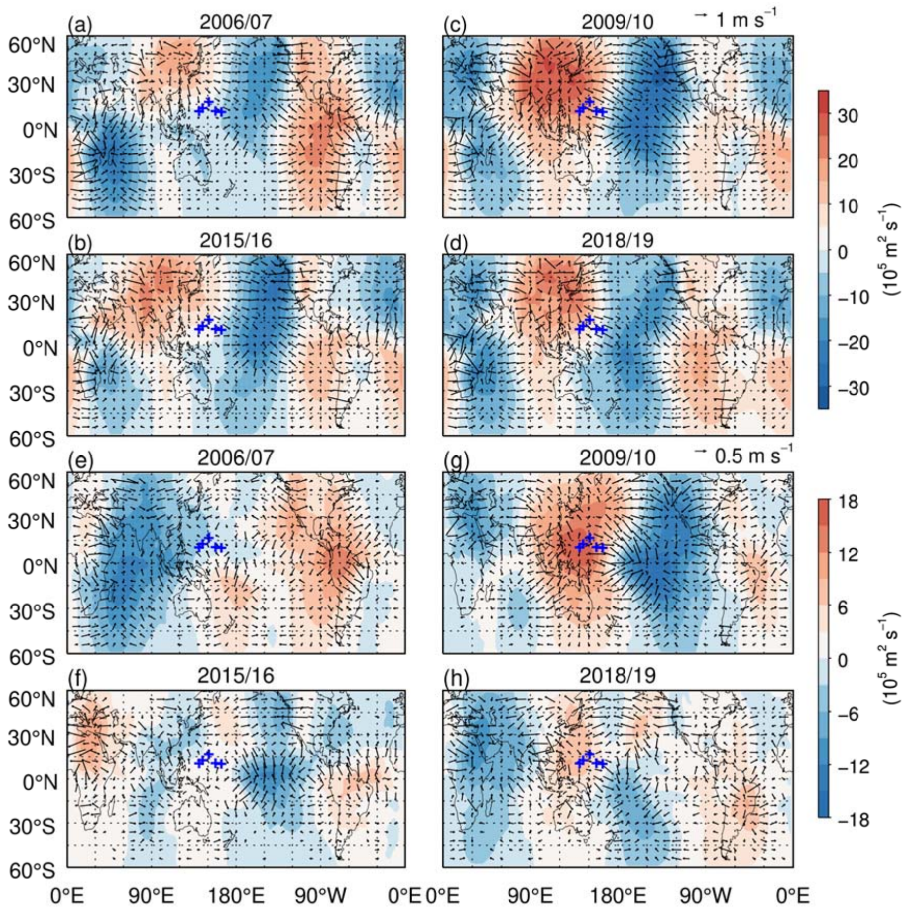

Figure 8. (shading) Velocity potential and (arrow) divergent wind of monsoon circulation and their anomalies at 850 hPa in (a, e) 2006/07, (b, f) 2015/16, (c, g) 2009/10 and (d, h) 2018/19 winters. Figure 8(a-d) denotes the velocity potential and divergent wind, and Figure 8(e-h) denotes their anomalies. The blue plus denotes the five radiosonde stations.

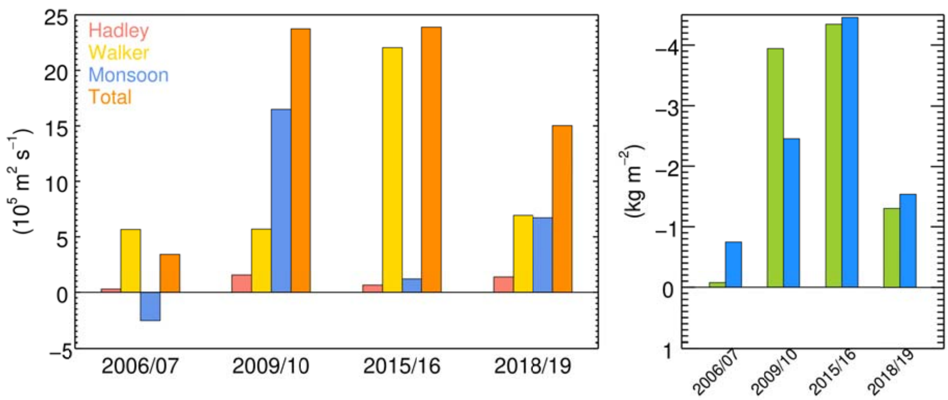

Figure 9. (Left) Indices of (red) Hadley, (yellow) Walker, (blue) monsoon and (orange) total circulation anomalies and (right) CWV anomalies derived from (azure) radiosonde and (green) reanalysis data at five radiosonde stations in four El Niño winters.

https://doi.org/10.5194/acp-2021-345
Preprint. Discussion started: 29 April 2021

Atmospheric Chemistry and Physics
Open Access
EGU
Discussions

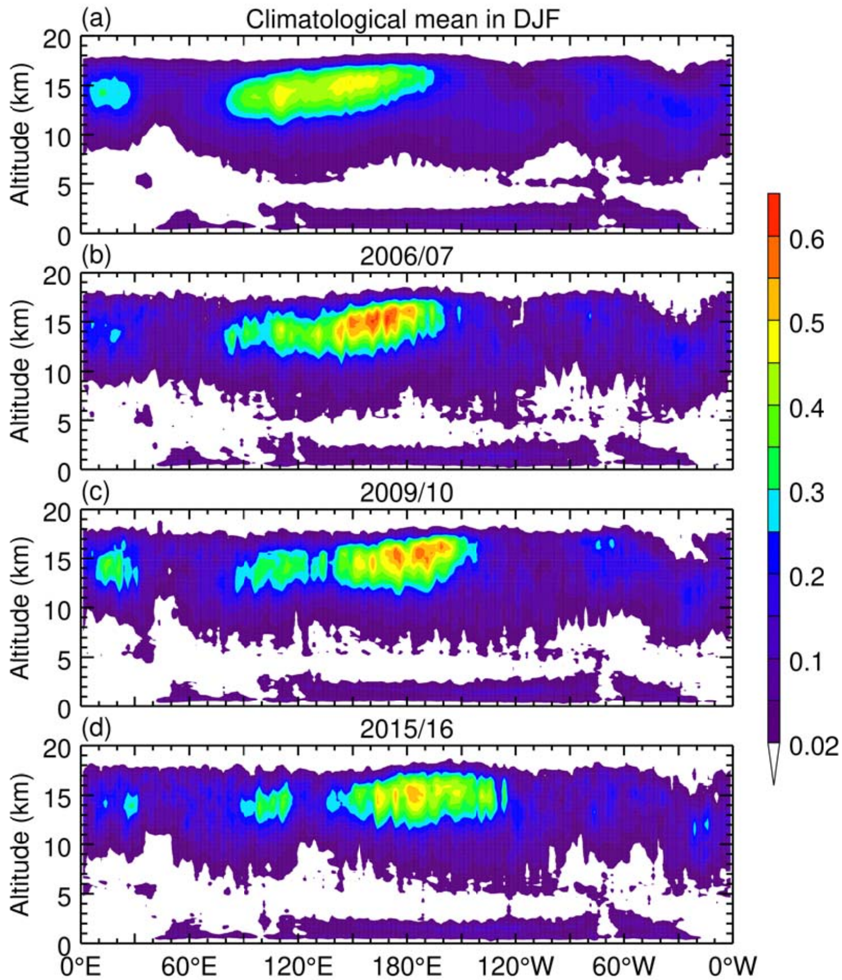

Figure 10. Distribution of cloud occurrence between 0°N and 15°N in (a) all winters, and (b) 2006/07, (c) 2009/10 and (d) 2015/16 winters derived from CALIPSO during June 2006 to December 2016.

https://doi.org/10.5194/acp-2021-345
Preprint. Discussion started: 29 April 2021

Atmospheric Chemistry and Physics Discussions

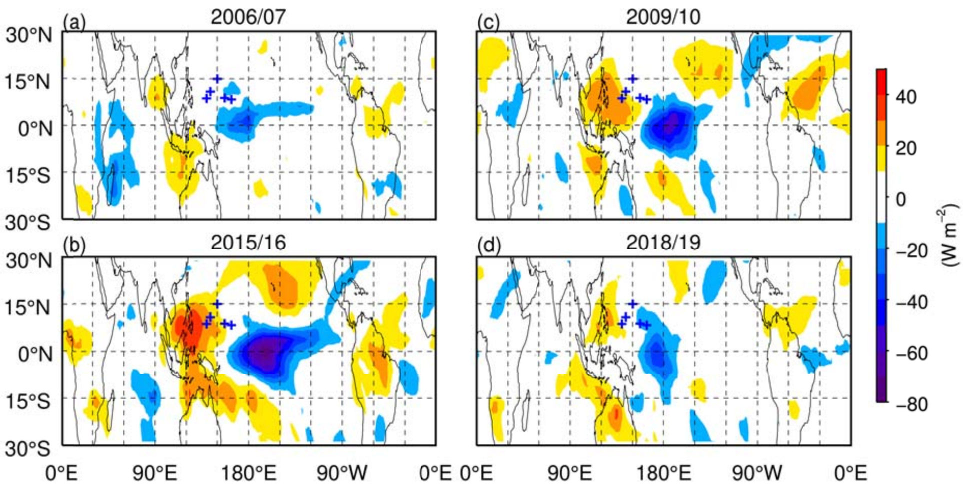

Figure 11. OLR anomalies averaged in (a) 2006/07, (b) 2015/16, (c) 2009/10 and (d) 2018/19 winters. The blue plus denotes the five radiosonde stations.